An Automated Experimentation System for the Touch-Response Quantification of Zebrafish Larvae

Yanke Wang, Daniel Marcato, Vani Tirumalasetty, Naveen Krishna Kanagaraj, Christian Pylatiuk, Ralf Mikut, Ravindra Peravali, and Markus Reischl

***Abstract*— Touch-response experimentation in zebrafish helps researchers better understand the link between genetics, drug effects, and behaviors. However, commonly manually conducted experimentation cannot fulfill a high-throughput screening and often delivers low accuracy and lacks reproducibility. Thus, the main aim of this work is to establish a fully automated robot-assisted experimentation system with minimal human participation to conduct the touch-response experimentation with freely swimming zebrafish larvae. Our designed system is able to undertake the role of repeated touch-response experiments at predefined specific location of the larvae in different ages and under different conditions, with high accuracy, robustness, and repeatability, and can also get comparable experimental results. The errors of the detection methods are less than 3 pixels and the offset errors of the touching points are less than 5%. Designed for high-efficiency experimentation, this system will promisingly release a great amount of the burden for the biological operators from touch-response experiments and may also have potential applications in other organisms for touch-evoked response analysis.**

***Note to Practitioners*—This article presented an automated touch-response experimentation system on zebrafish larvae, which can release a huge burden of the biological operators by achieving accurate, efficient, and repeated touch-response experiments. Manually conducted experiments are time-consuming and has low accuracy as well as difficult to do the quantification of the behaviors of the larvae. Our proposed system introduced an automated experiment pipeline and can also generate the behavior quantification of the larvae automatically, as the verification experiments confirmed. Basically, the research on the behaviors of zebrafish larvae requires large-scale data collection and analysis, so our system will play a vital role in such cases. Besides, the system can also be potentially used in other organisms, such as medaka larvae, and other related research, such as drug effects. In the current system, only one single larva was considered in each separate experiment, so our future work will be to achieve the experiments with multiple larvae in large scale for more high-throughput readouts and knowledge discovery.**

***Index Terms*— Biological experimentation system, image processing, touch-response quantification.**

Manuscript received 22 March 2021; revised 5 May 2021; accepted 6 August 2021. Date of publication 24 August 2021; date of current version 13 October 2022. This article was recommended for publication by Associate Editor X. Liu and Editor D. O. Popa upon evaluation of the reviewers' comments. This work was supported by China Scholarship Council (CSC). *(Corresponding author: Markus Reischl.)*

This work involved human subjects or animals in its research. Approval of all ethical and experimental procedures and protocols was granted by "Regierungspräsidium Karlsruhe" under Approval No. Az.35-9185.64, and performed in line with the European and national regulations and in accordance with the German law on Animal Protection and the Directive 2010/63/EU.

Yanke Wang, Christian Pylatiuk, Ralf Mikut, and Markus Reischl are with the Institute for Automation and Applied Informatics, Karlsruhe Institute of Technology, 76344 Karlsruhe, Germany (e-mail: markus.reischl@kit.edu).

Daniel Marcato was with the Institute for Automation and Applied Informatics, Karlsruhe Institute of Technology, 76344 Karlsruhe, Germany. He is now with Ditabis Digital Biomedical Imaging Systems AG, 75179 Pforzheim, Germany.

Vani Tirumalasetty, Naveen Krishna Kanagaraj, and Ravindra Peravali are with the Institute for Biological and Chemical Systems, Karlsruhe Institute of Technology, 76344 Karlsruhe, Germany.

I. Introduction

ZEBRAFISH larvae are regarded as an ideal and important biological model for studying the relationship between behaviors and the underlying genetic framework of an organism [1]. Zebrafish is commonly used in drug discovery to find new knowledge in the fields of biology and chemistry. In particular, a high-throughput screening of their behaviors is essential for statistically comparable outputs as well as reliable scientific conclusions. During the very early stage of development, zebrafish larvae have already established sensory and motor circuitry and respond to several stimuli including touching [2]–[6], tactile [7], startling [8], vibrational [9], visual [10]–[13], or chemical stimuli [14]. Particularly, the touch-response behavior has emerged to help in investigating the mechanisms underlying locomotion [3], learning and memory [15], as well as in identifying mutations [16]. Touch response is an escape response behavior of a zebrafish larva elicited by physical touching with a needle or the end of a regular Pasteur pipette or similar instruments [3]–[5]. This response is highly repeatable and distinguishable, as the response occurs similar to larvae under the same condition and is altered significantly in larvae exposed to neuroactive or neurodegenerative substances and in larvae that have sensory circuit and/or muscular mutations [2]. Consequently, understanding the touch-response behavior promises help in revealing the functioning of sensory and motor circuits along with the functioning of the neuronal architecture.

Conventionally, the "touching" is applied to zebrafish larvae manually and the response is captured in videos by using

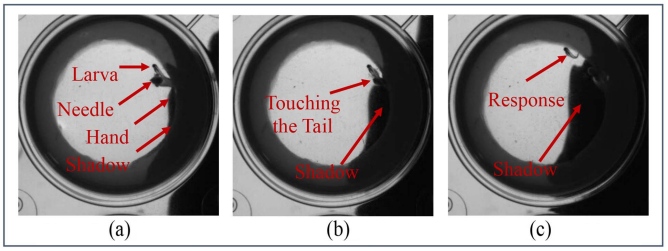

Fig. 1. Demonstration of touching the tail of the larva manually. (a) Before touching, the needle is moved close to the larva manually, and in this phase, the position of the needle is difficult to control and the larva may be touched accidentally. (b) Touching is conducted at the tail part of the larva manually. The touching position, angle, speed, and time are difficult to control by hand. (c) After touching, the larva has response immediately, and the beginning of the response may be not observable as the result of the shadows caused by the needle and hand.

a CCD camera or with a light microscope [6], [16]–[18]. However, the manual approach, as shown in Fig. 1 (as well as in Supplementary Material #M1, #M2, and #M3), has some obvious drawbacks, like high time consumption, low throughput, as well as lack of repeatability. Furthermore, the nature of this response is dependent on the location of the touch input on the zebrafish body and the force with which the touch input is applied. In manual experiments, nonetheless, these parameters cannot be strictly controlled for consistency and will show significant variations even by the same operator. Consequently, the response elicited may vary, thereby resulting in faulty conclusions. Furthermore, the hand or the needle may cause shadows that make the response of the larva not observable, or fluid motions that shock the larvae away, so the results in this way are usually not reliable and not comparable for specific conclusions or knowledge discovery. It is impossible to manually leverage the zebrafish model to scientifically perform high-throughput behavioral screening, so automated and intelligent systems need to be developed to accurately provide the touch stimulus, record the data at high speed and resolution, and automatically analyze the response behavior itself. For some other species, such as C. elegans, the automated systems have been developed to conduct touch-evoked experiments. For instance, systems using a microfluidic platform for C. elegans [19]–[22] limited the animal within a small area or even in a channel, causing the limitation of the movements of the animal but accelerating the experiment process. A much more precise system [23] was proposed to measure the force stiffness of specific parts of the C. elegans body in nano-scale level. As well, other systems were also proposed to conduct touch-evoke experiments on the freely moving C. elegans, like [24], which only focused on the mechanics of C. elegans to force-varied touching, and [25], in which the pair of permanent magnets still limited the movements of the animal and the touching angle cannot be well controlled.

So far, to the best of our knowledge, there are no automated systems that can be used to conduct touch-response experiments for zebrafish larvae. Common automated systems for C. elegans cannot be used for zebrafish larvae, as they have different size (2.5–3.7 mm from 30 to 96 hours post fertilization (hpf) [26]) from C. elegans (in micro scale [25]) in length. The design of an automated system for touch-response experiments faces several challenges and requirements: 1) minimal or no human intervention involved and high-throughput screening (recording the responses of a large number of larvae in a fast and unsupervised manner); 2) high accuracy and a good robustness (repeatability)—touching the same location of the larva and with the same speed (force) in each experiment; 3) comparable data acquired and automatically processed for readouts and potential conclusions; and 4) easily extended to other organisms and related experiments. Basically, the touch-response experiments of zebrafish can also be conducted in two ways as the experiments on C. elegans were done: 1) touching the fixed larva while observing brain activity (by using fluorescent reporters) [5], [17], [18], [27] or other tissues [28], [29] and 2) touching any anatomical positions as well as observing the response in freely swimming larva to understand the escape behavior itself and the kinematics [3]. The aim of our work is to study the locomotion behaviors of zebrafish larvae, so the second method is our focus.

In this article, we propose for the first time a fully automated touch-response system on freely swimming zebrafish larvae extended from our previous work [30]. This system uses a new image processing pipeline and new automatic behavior quantification methods and introduces a new touch-response experiment protocol. Based on image processing, we control a robot to touch a zebrafish larva with defined touching parameters [touching location, direction (angle), and speed (force)]. We analyze the behaviors of the zebrafish larvae by taking videos of the touch response and defining important readouts that can be generated automatically by using the behavior quantification methods. To evaluate the system, we analyze the accuracy and reproducibility of the detection algorithms and the distribution of the touched points. Using these readouts, we prove that the system can be used to quantify the influence of touching positions and the age as well as the impact of chemicals (drugs) on the response of the zebrafish. The design of this mechanical system not only promotes the development of the behavioral neuroscience research, but also contributes much in the field of robotics and automation regarding its technological design, the first use of automation technology on the study of the zebrafish model, new criteria and concepts of touch-response behavior quantification, and high repeatability of experiments for statistically scientific conclusions.

Organization of the article is as follows. Section II describes design structure, concepts, and image processing methods used in this system as well as the evaluation methods for them. Section III provides experiment pipelines, the accuracy and evaluation results of the designed system, and also details the statistical comparison of the behaviors of zebrafish to verify the effectiveness of the proposed system. According to the above results, conclusions are drawn in Section IV.

II. Touch-Response System Structure

The system designed works for data acquisition and analysis of the touch-response experimentation in an automated manner. Fig. 2(a) provides the pipeline of the whole system which is composed of four steps. Step 1 is the sample preparation where zebrafish larvae are obtained for the experiments, as discussed in detail in Section III-A. Step 2 is

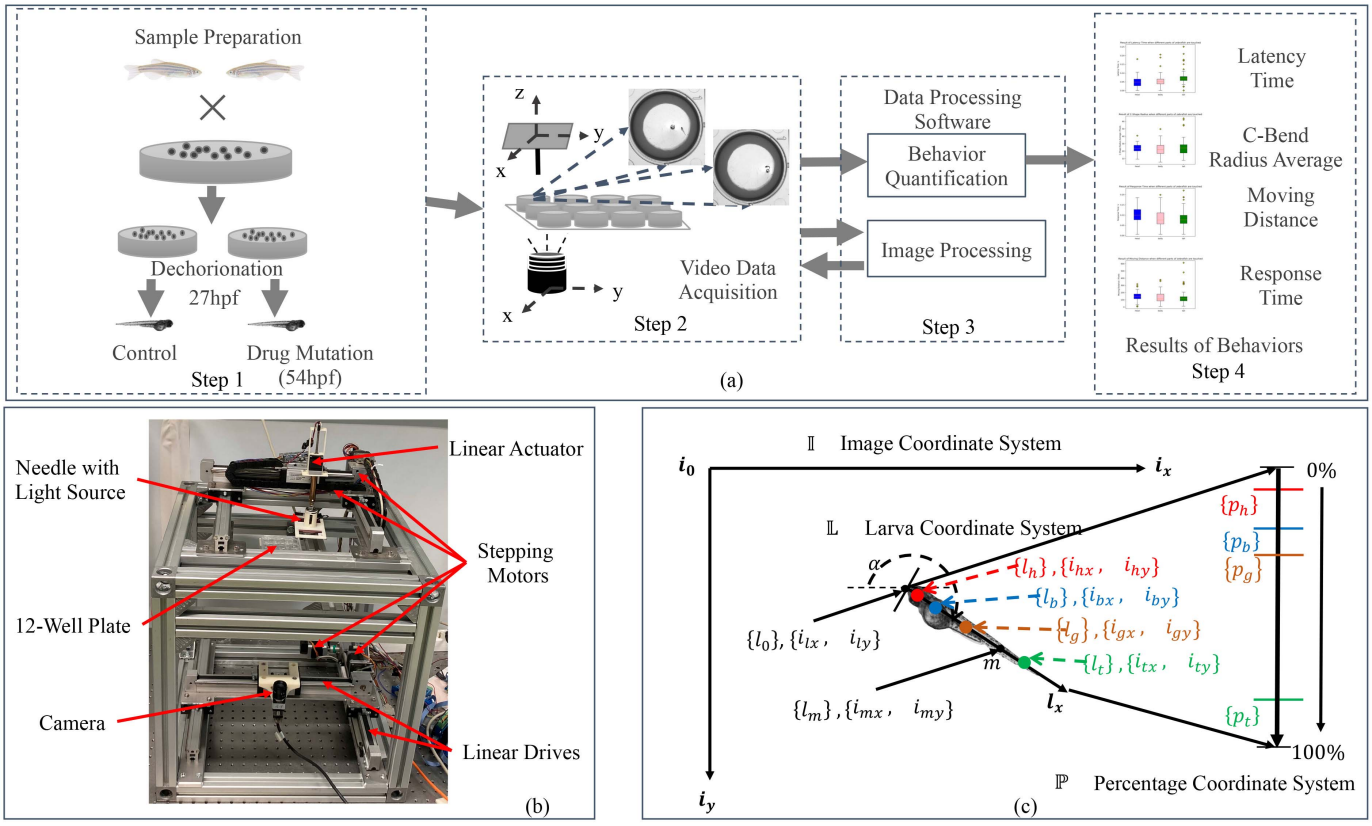

Fig. 2. (a) System architecture for the proposed touch-response system. Step 1. Preparation of the larvae used in the experiments according to a consistent protocol detailed in Section III-A. Step 2. Single larvae are mounted into each well and the blunt needle upright is moved between all wells to conduct the touch-response experiments, with videos of the larvae captured by a high-speed camera (objective Lensation CMFA1520ND). Step 3. Two sets of algorithms used, the image processing for the automatic experiments and data acquisition, and later on behavior quantification for analysis of the collected video data. Step 4. The processing of the videos results in four kinds of parameters, including latency time, C-Bend radius average, response time, and moving distance. (b) The real image and main components of the designed system, detailed in Section II-A. (c) Three coordinate systems were established: the image, larva, and percentage coordinate systems ($\mathbb{I}$, $\mathbb{L}$, and $\mathbb{P}$). The origin of $\mathbb{I}$ is the first pixel at the top-left of the image, and the origin of $\mathbb{L}$ at the head beginning point of the larva. Also, the larva is scaled in the range of [0%, 100%] as $\mathbb{P}$, with three predefined touching points for head (in red), body (in blue), and tail (in green) as $\boldsymbol{p_h}$, $\boldsymbol{p_b}$, and $\boldsymbol{p_t}$.

the actual touch-response system for video data acquisition, which operates on the samples obtained from Step 1. The designed system automatically conducts the touch-response experiments and outputs the collected video data based on image processing algorithms (indicated in Step 3). Also, based on behavior quantification algorithms in Step 3, Step 4 obtains relevant readouts and provides a statistical analysis of the results. Fig. 2(b) vividly displays the main components of the proposed system, and the individual concepts used in this system will be further discussed below.

A. System Design

The system is composed of a blunt needle for applying the touch input, a microtiter (well plate), a high-speed camera, and a data processing software [Step 2 and Step 3 of Fig. 2(a) and (b)]. In order to give the larva enough space to move and also to collect as many videos as possible, we chose a 12-well plate with one larva in each well and added an agarose ring at the edge of each well to keep the larva inside the view. The video capturing and needle touching should be conducted at the same time, so the needle mounted with a light source was set over the well plate with the camera under the well plate [displayed in Fig. 2(b)]. They are both controlled by the actuator systems correspondingly described in Section II-B4. The experiments are conducted repeatedly by moving the needle and the camera to each target well one by one, with resulting videos captured by the camera for later-on analysis.

B. Concepts

1) Experiment Subject: The aim of the system is to evoke a response to a touching input on zebrafish larvae. The zebrafish model is amenable to high-throughput experiments owing to the high fecundity. Zebrafish larvae develop very rapidly and start responding to touching at about 21 hpf when they are still inside the chorion (egg shell) [8] by demonstrating vigorous body coiling. The larvae hatch between 48 and 72 hpf [26]. At this age, they do not exhibit spontaneous locomotion and there is no movement before the application of tactile stimuli or with minor mechanical stimuli. However, when subjected to touching, they show an escape response which consists of three components: a bending of the body into a C-Bend, a reverse C-Bend, and a swimming bout to escape from the position where the input was applied [8]. Therefore, zebrafish larvae from 30 to 78 hpf (dechorionated at 27 hpf) were used to do the touch-response experiments by our system. Furthermore,

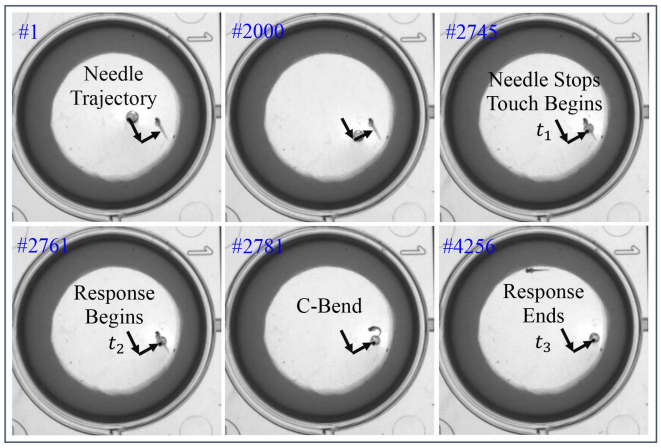

Fig. 3. Sequence of key frames (with frame number in blue) in one video collected in a tail touching experiment. The black arrow line is the moving trajectory of the needle (details in Section II-C). The touching input is applied at #2745, and the response happens from #2761 to #4256. The C-Bend, for an example, is visualized at #2781.

the embryos are contained in a well plated with 2.5 mL of medium (in Table I), which ensures that the movements of the larvae are essentially restricted to 2-D.[1]

2) Coordinate System: In touch-response experiments, the larvae may respond differently with different anatomical points[2] touched: the head, the body (trunk of the larvae), or the tail as shown in Fig. 2(c). Therefore, the image and larva coordinate systems were predefined (shortened as $\mathbb{I}$ and $\mathbb{L}$) in Fig. 2(c), where α is the orientation angle of the larva in $\mathbb{I}$. The coordinates in image coordinate system are formulated as $\boldsymbol{i_*} = \{i_{*x}, i_{*y}\}$ with the origin as $\boldsymbol{i_o}$, and the coordinates in larva coordinate system are formulated as $\boldsymbol{l_*} = \{l_*\}$ with the origin as $\boldsymbol{l_o}$. Assumed that the origin of $\mathbb{L}$ is expressed as $\boldsymbol{i_l} = \{i_{lx}, i_{ly}\}$ in $\mathbb{I}$, a point m ($\boldsymbol{l_m} = \{l_m\}$ in $\mathbb{L}$), for example, could be transferred to $\mathbb{I}$ as follows:

$$\boldsymbol{i_m} = \begin{bmatrix} i_{mx} \\ i_{my} \end{bmatrix} = \boldsymbol{T_L^I} \boldsymbol{l_m} = \begin{bmatrix} -\cos\alpha & i_{lx} \\ -\sin\alpha & i_{ly} \end{bmatrix} \begin{bmatrix} l_m \\ 1 \end{bmatrix} \tag{1}$$

where $\boldsymbol{T_L^I}$ is the transformation matrix from $\mathbb{L}$ to $\mathbb{I}$. To formulate the touching points, the larva is mapped in the range of [0%, 100%] as percentage coordinate system $\mathbb{P}$, with the head beginning point at 0% and the tail ending point at 100%. The percentages in $\mathbb{P}$ are formulated as $\boldsymbol{p_*} = \{p_*\}$ with the origin as $\boldsymbol{p_o}$. Ideally, it is possible for the system to touch any region of the larva, and to clearly show the performance of the system, the three touching points are defined in $\mathbb{P}$ ($\boldsymbol{p_h}, \boldsymbol{p_b}, \boldsymbol{p_t}$) with corresponding coordinates in both $\mathbb{L}$ ($\boldsymbol{l_h}, \boldsymbol{l_b}, \boldsymbol{l_t}$) and $\mathbb{I}$ ($\boldsymbol{i_h}, \boldsymbol{i_b}, \boldsymbol{i_t}$).

3) Experiment Criteria: Many unanswered questions could be revealed by the locomotor behaviors of zebrafish larvae during response to stimuli, which needs collaborative work of a variety of cell or neuron types. The tail touching experiment, for example, is conducted as listed in a sequence of Fig. 3. In total, we describe four parameters to be estimated to quantify the larva behaviors. Throughout the experiment, three time points of importance are: 1) the time at which needle stops and touch begins (t_1, #2745 in Fig. 3); 2) the time at which response begins (t_2, #2761); and 3) the time at which response stops (t_3, #4256). The first parameter to be estimated is the latency time (t_l) before response: The larva takes some time to respond after being touched ($t_l = t_2 - t_1$). During the response, the larva shapes into a C-Bend [31] between t_2 and t_3 (as #2781 shows), and the amplitude of it indicates the strength of the larva's response. Thus, the average radius of the C-Bends during the whole response is also quantified. Moreover, the response time ($t_r = t_3 - t_2$) and total distance of the larva moving also differ under various stimuli [32], [33]. To summarize, this quantification involves latency time, C-Bend radius average, response time, and moving distance, which will potentially help construct a working model that represents the response pattern of zebrafish to touching or other stimuli. How to achieve the quantification methods is detailed in Appendix D.

4) Actuator System: The actuators used in the system include four stepping motors (ST4118L1804-B–STEPPER MOTOR–NEMA 17, Nanotec – Munich) and one linear actuator. Two stepping motors, mounted by two linear drives (Der isel – Zahnriemenvorschub LEZ 1, Germany) orthogonally, work together to move in the 2-D plane and the linear actuator is used to achieve the movement in the z-axis [as shown in Fig. 2(b)]. Besides, two switches are fixed at the initial and end positions of each actuator for providing a correct positioning as well as for the safety of the actuators. Each stepping motor moves 1.8°/step, and the translational distance is 0.3 mm/step. Additionally, each full step is subdivided into 16 microsteps to be well controllable.

C. Image Processing

Image processing is used to detect the needle and different parts of the zebrafish larva and thus to generate touching trajectories. Therefore, we aim to robustly segment needle and larva, based on the introduction of a larva-centered coordinate system [$\mathbb{L}$, seen in Fig. 2(c)], which is used to define touching points of the larva and trajectories. As mentioned in Section II-B1, we characterize early embryonic and eleutheroembryonic stages of zebrafish larvae where they are still immotile and do not exhibit any spontaneous locomotion. Movements are elicited only with tactile inputs and are reflective of the developmental processes in an organism. Thus, this means that we do not need image processing a second time after the larva and the needle were detected for each well.

To begin with, a circle Hough transform [34] is used to crop the image within the target well, as shown in Steps 1 and 2 of Fig. 4. Afterward, two objects should be detected. The first one is the needle which is the darkest part of the image in most cases. Thus, a binarization with a lower heuristic threshold (T_n) is used to find the needle area, probably with some noise caused by such as uneven distribution of the light and the larva. In most cases, however, the noise is smaller than the needle

[1]Zebrafish larvae normally start swimming in 3-D after six days post fertilizations.

[2]In this study, all zebrafish larvae used were raised and collected in conformity with the Animal Ethical Requirements.

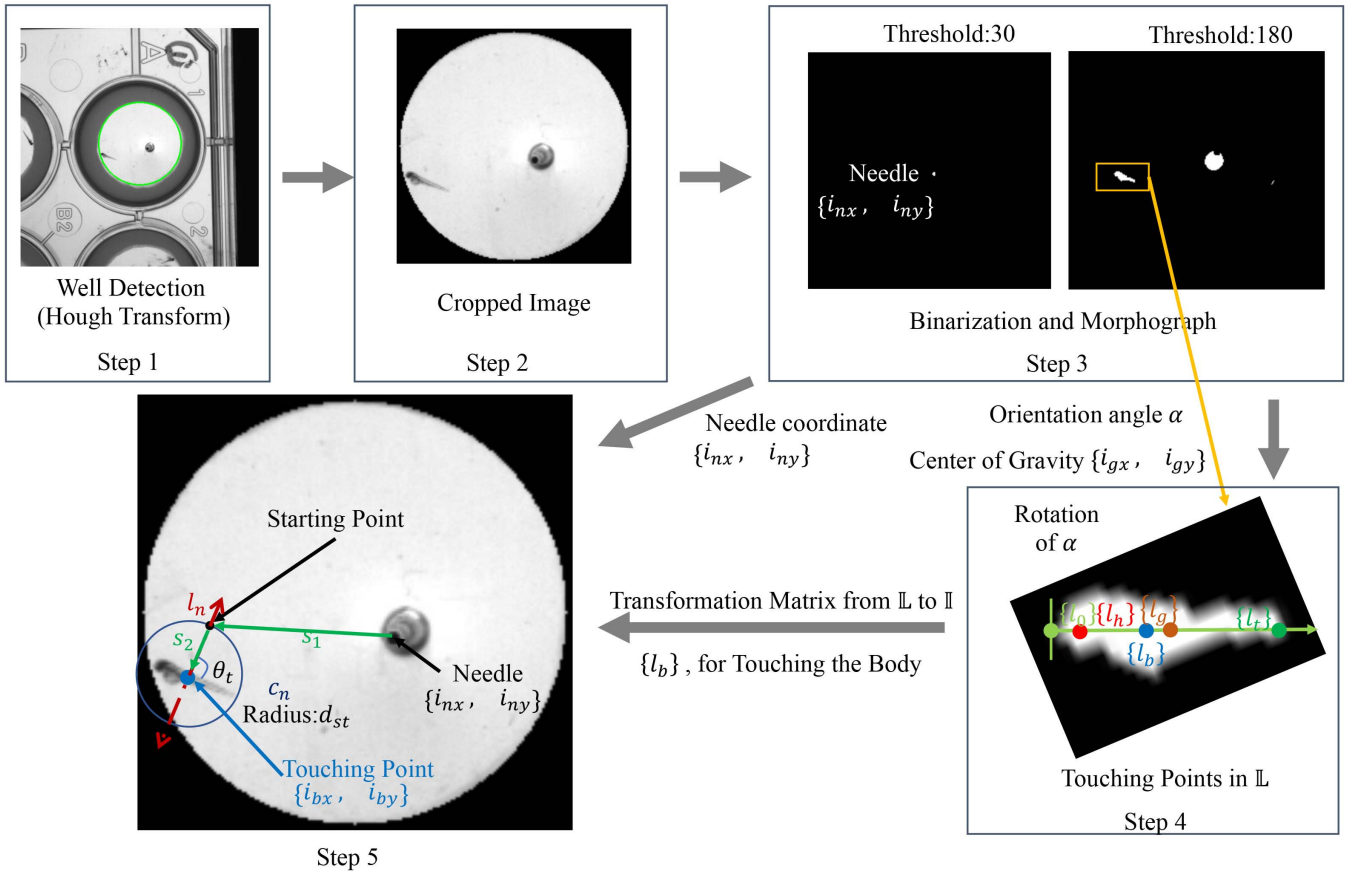

Fig. 4. Pipeline of image processing. Step 1. Hough Transform for cropping the image within the well, with result shown in Step 2. Step 3. Binarization used for needle and larva detection, with threshold being 30 and 180, respectively. Step 4. The rotated larva with an orientation angle of α. Each touching point is mapped to $\mathbb{L}$, which is transformed to $\mathbb{I}$ by using the transformation matrix. Step 5. An example of the trajectory generation for touching the body. The coordinates of the body are marked in blue, whereas the trajectory in green.

to be easily filtered. The position of the needle is computed as the center of gravity of the found area $\boldsymbol{i_n} = \{i_{nx}, i_{ny}\}$ in the image coordinate system.

The second object to detect is the larva, which is more difficult as it is transparent and relatively small with only a few pixels in the whole image. The head, body, and tail of the larva are required to be detected. Binarization with a higher heuristic threshold (T_l) is applied to the cropped image, and the resulting binary image contains two objects (the needle and the larva) and some noisy areas, which is optimized by morphology (kernel size mentioned in Table I) to find the closing objects seen in Step 3 of Fig. 4. Here, the two biggest areas are the needle and the larva, so we can locate the area of the larva as the position of the needle is already known. From this area, orientation angle α [in the range of $(-180°, 180°)$] of the larva is calculated. After a rotation of α, as shown in Step 4 of Fig. 4, the center of gravity $\boldsymbol{l_g} = \{l_g\}$ in $\mathbb{L}$ is computed by averaging the coordinates of the whole detected larva area. Besides, the head part of the larva has more pixels than the transparent tail part, so the center of gravity of the larva is closer to the head part. With the rotation range α, the head beginning point of the larva is rotated to the left side, as $\boldsymbol{l_o} = \{l_o\}$ in $\mathbb{L}$, and three touching points of the larva—head, body, and tail in the larva coordinate system—are decided by using a fixed ratio as follows:

$$l_h = (l_g - l_o) \times \frac{p_h}{p_g} \tag{2}$$

$$l_b = (l_g - l_o) \times \frac{p_b}{p_g} \tag{3}$$

$$l_t = (l_g - l_o) \times \frac{p_t}{p_g} \tag{4}$$

where $\{p_h\}, \{p_b\}, \{p_t\}$ are the coordinates of the head, body, and tail of the larva in $\mathbb{P}$, respectively (predefined as shown in Table I), and $\{l_h\}, \{l_b\}, \{l_t\}$ are the corresponding coordinates in $\mathbb{L}$, respectively. These three touching points (head, body, and tail) of the larva are then transformed from $\mathbb{L}$ to $\mathbb{I}$ according to the transformation matrix mentioned in Section II-B2.

Having detected the larva, we need to generate a touching trajectory and control the motors correspondingly. In order to touch the larva in the same angle and speed for each experiment, a two-step moving strategy was designed from the needle point to a defined starting point, then to the touching point (the fish part). Both the touching angle θ_t and the distance between the starting point and the touching point d_{st} are predefined. To compute the starting point, a line l_n is defined, crossed with the skeleton of the larva with the angle θ_t at the touching point, as shown in Step 5 of Fig. 4. Afterward,

a circle c_n around the touching point is also defined with a radius being d_{st}. The crossing between l_n and c_n generates two points, the closer one of which to the needle is the starting point. Additionally, the speed of moving needle from the needle point to the starting point is set at s_1 and then to the touching point at s_2.

D. Evaluation Method

The needle and larva detection methods are the key of the proposed automated touch-response system. For the accuracy of them, the locations of the center (needle and larva) are of importance. Therefore, the error between manually labeled ground-truth center (as $\{i_{Cgx}, i_{Cgy}\}$) and detected center (as $\{i_{Cdx}, i_{Cdy}\}$) is calculated as

$$e_{gd} = \sqrt{(i_{Cgx} - i_{Cdx})^2 + (i_{Cgy} - i_{Cdy})^2}. \tag{5}$$

Additionally, the detected area of the larva is also vital to find out the center of gravity and orientation of it. Assuming the detected bounding box of the larva is B_d, its ratio of overlap (R_o) with labeled ground-truth box B_g is computed as follows:

$$R_o = \frac{A\{B_d \cap B_g\}}{A\{B_g\}} \tag{6}$$

where $A\{*\}$ is the area of the bounding box. Generally, the threshold (T_o) of R_o is defined to decide whether the larva is successfully detected (recalled). R_o gives the "degree" of how the detection output covers the ground-truth box. Thus, the threshold (T_o) of R_o is the minimum "degree" deciding whether the detection output is successful. For vivid demonstration, the ratio of recall (R_r) of the larva detection is also defined with T_o fixed, as follows:

$$R_r = \left.\frac{N_d}{N_g}\right|_{T_o} \tag{7}$$

where N_d is the number of the successfully detected larvae, and N_g is the number of the ground-truth larvae that are expected to be detected.

III. Experimentation and Results

A. Experimental Setup

Three sets of verification experiments were conducted on the zebrafish larvae: 1) experiments on three larva parts (E_p)—the influence of touching points; 2) experiments on ages (E_{db})—analysis of their development according to response; and 3) experiments on treatments (E_{tb})—the influence of the treatments on their behaviors. The protocol of these experiments is shown in Appendix C. Normally, the zebrafish larva hatches on the third day (around 72 hpf), so the larva was dechorionated (at 27 hpf during the first day, 3 h before the experiments) as described in Appendix C. The detailed experimental setup is as follows.

1) The experiment E_p was conducted by touching the head, body, and tail ($p_h = 5\%$, $p_b = 30\%$, $p_t = 65\%$ as listed in Table I) of the controls at only 54 hpf.

TABLE I
Parameters Used in the Experiments

Parameters	Value
Image size	480 × 480 pixels
Diameter of well plate	22.1 mm
p_h	5%
p_b	30%
p_g	30%
p_t	65%
Frame rate	1000 FPS
Maximum length of videos	10s
Volume of water in each well	2.5 mL
T_n	30 pixels
T_l	180 pixels
T_m	20%
Morphology kernel size	5×5
θ_t	90°
d_{st}	30 pixels
s_1	80 steps/s
s_2	400 steps/s
Number of controls	12
Number of treated larvae	12

2) The experiment E_{db} was conducted by touching the body of the controls, and three time points were considered, including 30, 54, and 78 hpf.
3) As for the experiment E_{tb}, larvae were treated with Tricaine (an anesthetic) at 54 hpf and taken out from the treatment after 60 min at 55 hpf, and the experiments were conducted every 30 min by touching the body of the controls and treated larvae at 54, 54.5, 55, 55.5, 56, 56.5 hpf, respectively.

For each collected video, the maximum length is 10 s. Thresholds and filter size used in image processing are also outlined in Table I. In addition, to introduce less changing factors, we fixed θ_t at 90°, s_1 at 80 steps/s (lower speed to not shock the larva) and s_2 at 400 steps/s (higher speed to simulate the response), which were selected heuristically to not generate flow disturbance or vibration of water. The distance between the starting point and the touching point was set to 30 pixels also in order to not shock the larva before touching. The graphical user interface (GUI, shown in Appendix A) of the system together with image processing used in this system was coded in C#, and the behavior quantification algorithms were implemented offline by Python.

B. Evaluation of the Touch-Response System

To evaluate the methods of detection mentioned in Section II-C, we collected an evaluation dataset (806 videos, as DA-I) and used the first frame of each video (with manual annotations) to quantify the performance of these methods according to the evaluation methods in Section II-D. The center errors e_{gd} of the needle and larva detection are shown in Table II, and the R_r with respect to T_o of R_o is drawn in Fig. 5(a). Both e_{gd} are less than 3 pixels, which ensures an accurate detection of the needle and larva. The ratio of recall

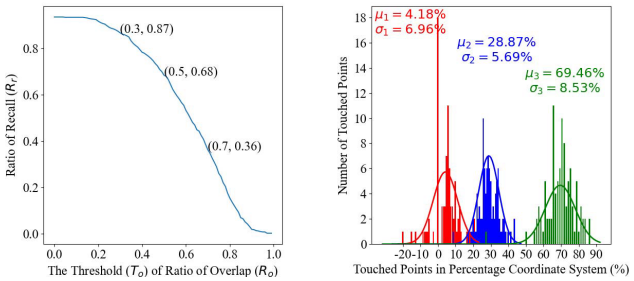

Fig. 5. Evaluation of the system. (a) Ratio of recall of larva detection with respect to T_o on DA-I. According to (7), the threshold of R_o could be chosen for successful recall of the larva detection, and the ratio of recall drops with the increase of this threshold. (b) Distribution of the touched points with the proposed system tested on DA-III. The touched points are mapped to $\mathbb{P}$ (seen in Fig. 2(c), red for the head, blue for the body, and green for the tail). The x-axis is the percentages of the touched points in $\mathbb{L}$, with the y-axis being the frequency (number). Three optimized normal distributions show the robustness of the touching task, with their means and standard deviations.

TABLE II
RESULTS OF EVALUATION METHODS

Evaluation Method	Value
e_{gd} for needle on DA-I (pixels)	1.04
e_{gd} for larva on DA-I (pixels)	2.64
Hardware error on DA-II (pixels)	2.52
Head touched point error on DA-III (%)	0.82
Body touched point error on DA-III (%)	1.13
Tail touched point error on DA-III (%)	4.46

[according to (7)] is between 90% and 100% when $T_o \leq 0.3$ and decreases significantly from $T_o = 0.5$ and converges to 0 after $T_o \geq 0.9$ (more evaluation in Appendix B). Combined with the result of e_{gd} in Table II, we can see that the detection methods could ensure an accurate location of the larva with error less than 3 pixels. However, the tail part of the larva is not that easy to be found, as it is the most transparent part, so our methods may lose some information of the larva with a low ratio of recall in Fig. 5(a). Thus, it is reasonable and practical to locate the different parts of the larva by using (2) to (4). Apart from the errors from the detection methods, the hardware of the system (stepping motors) also result in some error (hardware error) and we calculated it by moving the stepping motors to 12 random points (as DA-II), and the results are shown in Table II.

To evaluate the repeatability of this system for touching tasks, by using 300 videos (as DA-III), touched points in $\mathbb{P}$ were analyzed by comparison with the predefined touching points (p_h, p_b, p_t) in Table I. These touched points are figured as a histogram in Fig. 5(b), including their corresponding fit normal distributions (with mean μ and standard deviation σ). The accuracy of three parts touching is also shown in Table II, which is computed by the difference between predefined touching points in Table I and the mean of the distributions of the touched points (μ_1, μ_2, μ_3) in Fig. 5(b). The head touching has the highest accuracy with touched point error being 0.82%, the body touching has an accuracy of 1.13%, and

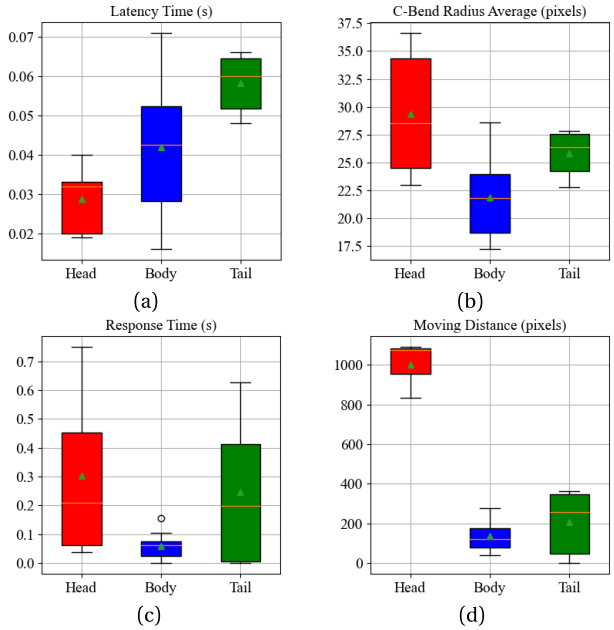

Fig. 6. Results of the behavior quantification on DA-IV with different points touched at 54 hpf of the larvae, including four quantification indexes: latency time, C-Bend radius average, response time, and moving distance. (a) Latency time. (b) C-Bend radius average. (c) Response time. (d) Moving distance.

the tail touching has an accuracy of 4.46%. The robustness of three parts touching can also be observed from the standard deviations of the fit normal distributions in Fig. 5(b). The body touching has a better robustness than the other two, and the tail touching is still the worst with the highest standard deviation. These three parts are clearly in different positions of the larva, thereby leading to comparable inputs to the experiments compared with manually touching. In addition, the repeatability of the touching tasks is shown by $\sigma_1, \sigma_2, \sigma_3$ in Fig. 5(b), the tail touching has the least repeatability ($\sigma_3 = 8.53\%$ compared with $\sigma_1 = 6.96\%, \sigma_2 = 5.69\%$ of the head and body touching) since the center of gravity may be slightly disturbed because of the transparent tail part. A small error at the center of gravity may be enlarged at the other two parts as a result of (2) to (4).

C. Touch-Response Analysis With Different Touching Parts

The zebrafish larva's response may be dependent on the touched anatomical points; thus, to verify this hypothesis, we acquired 36 videos (touching the head, body, and tail of 12 controls at 54 hpf, as DA-IV, see examples in Supplementary Material #A2, #A3, and #A4) using our systems.

For the behavior analysis during response, Fig. 6 displays the difference between each touching point, including four quantification indexes: latency time, C-Bend radius average, response time, and moving distance. As the result of latency time in Fig. 6(a) shows, the head touching caused the quickest response of the larvae and the tail touching caused the slowest response. Fig. 6(b) shows the result of the averaged radius of the C-Bends that the larvae shaped, which gives a clue of the strength (amplitude) of their response. The larvae with head and tail touched responded in C-Bend with a larger

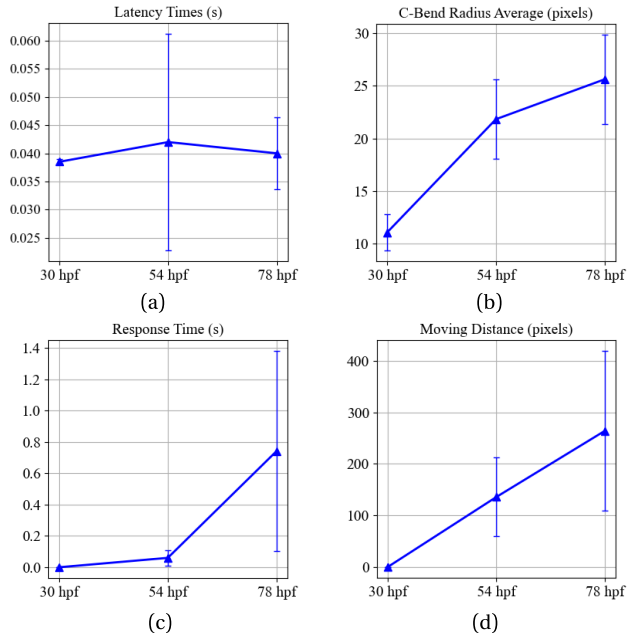

Fig. 7. Temporal line charts of the behavior quantification on DA-V with the body touched at 30, 54, and 78 hpf of the larvae. (a) Latency time. (b) C-Bend radius average. (c) Response time. (d) Moving distance.

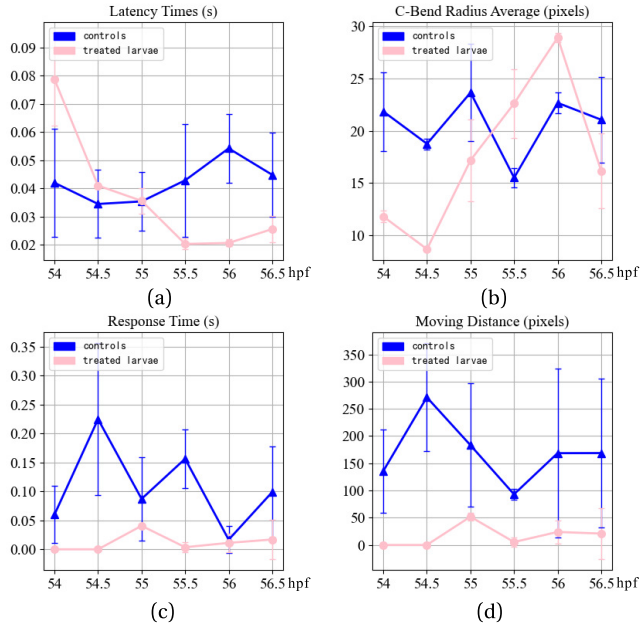

Fig. 8. Results of the behavior quantification on DA-VI with the body touched at 54, 54.5, 55, 55.5, 56, and 56.5 hpf of the controls and treated larvae, including four quantification indexes: latency time, C-Bend radius average, response time, and moving distance. (a) Latency time. (b) C-Bend radius average. (c) Response time. (d) Moving distance.

radius compared with the body touching stimuli. The larger the radius is, the less the strength of the response is, so the larvae having body touching stimulus had a higher response amplitude. Besides, Fig. 6(c) and (d) shows the results of response time and moving distance during the whole response. These two results are consistent, more response time with more moving distance. In short, the head touching caused the larva a quick and lasting response, but the body touching made the larva respond more strongly but less lasting. The results above verify that different inputs of the touching points could bring valid and comparable readouts.

D. Touch-Response Analysis With Different Ages

The development of the larvae may also influence the behaviors of the larvae. In this case, we collected 36 videos (touching the body of 12 controls at 30, 54, 78 hpf, respectively, as DA-V, see examples in Supplementary Material #A1, #A3, and #A6) based on our system.

Verification results could be observed in Fig. 7. The line charts with corresponding mean value (blue triangle) and error bar display the tendency of four quantification indexes (latency time, C-Bend radius average, response time, and moving distance) with the development of the larva. Fig. 7(a) shows no significant changes in latency time with the larva growing older, and Fig. 7(b)–(d) describes a consistent trend, older larvae (78 hpf) responded with less amplitude (larger C-Bend radius) but longer lasting (more response time and moving distance) compared with younger larvae (30 and 54 hpf). These comparable experimental results confirm that the ages of the larvae are an important factor to their touch-evoked response and that our system could also take the role of touch-response behavior analysis in such case.

E. Comparison of Touch Response Between Controls and Treated Larvae

As indicated in many previous studies on zebrafish [2], [14], [16], chemicals or drugs were commonly used for the changes of the behaviors of zebrafish. In order to verify the performance of our system on experiments between controls and chemically treated larvae (detailed in Section III-A), 144 videos (as DA-VI, see examples in Supplementary Material #A3 and #A5) were collected by touching the body of 12 controls and 12 treated larvae at 54, 54.5, 55, 55.5, 56, and 56.5 hpf, respectively. The treated larvae were expected to not move within the treatment (being anesthetized) and begin to wake up after taken out from the treatment, and the controls were assumed to have no obvious behavior changes during such period of time. The line charts of four quantification indexes in Fig. 8 verify our assumption. The response of the controls differs only slightly from 54 to 56.5 hpf, but the treated larvae scarcely had response within the treatment (at 54 and 54.5 hpf) and began to respond more quickly (less latency time), less strongly (higher C-Bend radius average), and more lasting (more response time and moving distance) after taken out from the treatment (at 55 hpf). The results above still provide a verification that our system could play a role in the analyzing behavior changes of the larvae under treatment.

IV. Conclusion

In this article, we presented an automated touch-response experimentation system based on image processing. The presented system works, with minimal human participation, to carry out touch-response experiments as well as analyze the

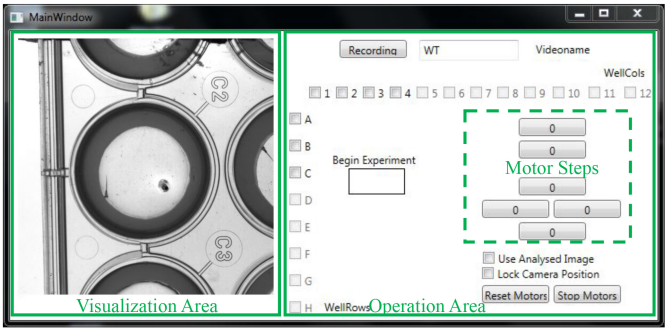

Fig. 9. GUI used in the touch-response experimentation system.

results automatically. The proposed image-processing methods finished the detection work with less than 3 pixel errors, and the touching tasks were fulfilled with less than 5% offsets of the expected touching points. As three verification experiments (experiments on three parts, three ages, and treatment) confirmed, this system has high accuracy and robustness, and repeatability. In these verification experiments, this system worked as expected to input valid and specific touching inputs to the experiments, so more experiments on other locations (percentages) of the larva can also be carried out by the proposed touch-response system accordingly. Besides, further experiments with our system are needed to study other stages of development of the larvae. In such case, our proposed system is expected to take a vital role in acquiring large-scale data from these repeated experiments. Finally, although we only considered one treatment with one concentration, more experiments can be further conducted to find out the influence of other drugs (or compounds) on zebrafish's behaviors, such as the concentration of them. In these experiments, statistical analysis on large-scale data is also of vital importance, in which our designed system is also essential to help. Our future work will be, based on these experiments, to build a statistical model between the changes of the touch-evoked response and the input stimuli on zebrafish larvae.

Appendix A
Graphical User Interface

The GUI contains two main areas: the visualization and operation area (as shown in Fig. 9). In the visualization area, the video captured by the camera is shown in real time when the motors move, and the "Motor Steps" of the GUI also visualizes how many steps the motors move on. In the operation area, there are a group of buttons (1–12 in columns, A–H in rows). Specific target wells can be selected by the click of these buttons. The "Begin Experiment" button is used to start the experiments. The "Stop Motors" button is designed for stopping the experiments during the process. After experiments are finished, the "Reset Motors" button can be used to reset the whole system.

Appendix B
Evaluation of Larva Detection Method With Intersection Over Union

Besides the ratio of overlap (R_o) mentioned in Section II-D, intersection over union (IoU) is also commonly used for the evaluation of detection methods. As defined in Section II-D, the detected bounding box of the larva is B_d, so its IoU with labeled ground-truth box B_g is computed as follows:

$$\text{IoU} = \frac{A\{B_d \cap B_g\}}{A\{B_d \cup B_g\}} \tag{8}$$

where $A\{*\}$ is the area of the bounding box. Similarly, the ratio of recall (R_r) with IoU is also defined as (7) in Section II-D, with result shown in Fig. 10. The ratio of recall with IoU is slightly lower than that with R_o when T_o is over 0.5, which supports the result and conclusion in Section III-B. As we aim to evaluate the "degree" of how the detection result covers the ground-truth box, ratio of overlap (R_o) is used in Sections II-D and III-B.

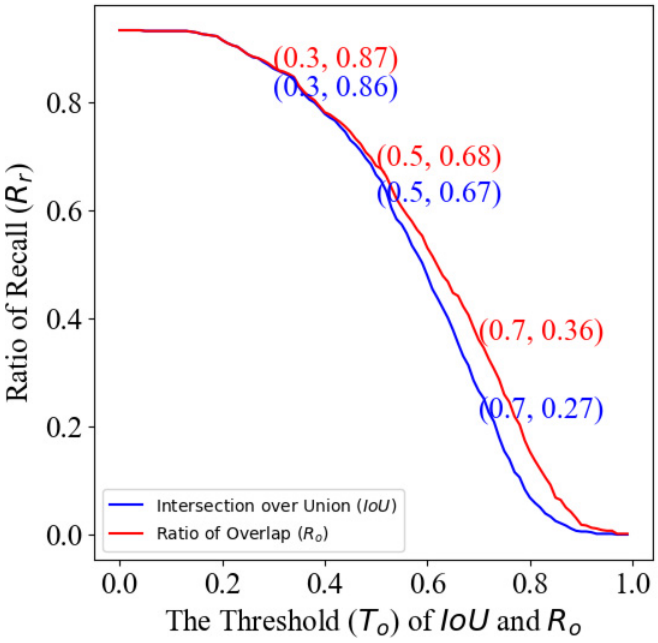

Fig. 10. Ratio of recall of the larva detection with respect to T_o of IoU (in blue) and R_o (in red), evaluated on DA-I.

Appendix C
Experimental Protocol

As mentioned in Section III-A, three sets of experiments (E_p, E_{db}, E_{tb}) were conducted (as shown in Fig. 11). In each experiment, 4 mL of agarose was added to each well and then a ring of agarose was cut out at the edge of the well. The volume of the fish water was 2.5 mL and speed to touch the larva s_2 was set 400 steps/s. Basically, the embryos were collected at 9:00 A.M. one day after crossing as 0 hpf and were dechorionated at 27 hpf, since the experiments were conducted even before they normally hatched (around 72 hpf). For E_{db}, the body of 12 controls was touched every 24 hpf from 30 to 78 hpf, and for E_p, 12 controls were used to touch their head, body, and tail at 54 hpf. As for E_{tb}, the treatment was added to 12 larvae at 54 hpf for 60 min and the experiments were conducted on these 12 treated larvae and another 12 controls every 30 min from 54 to 56.5 hpf.

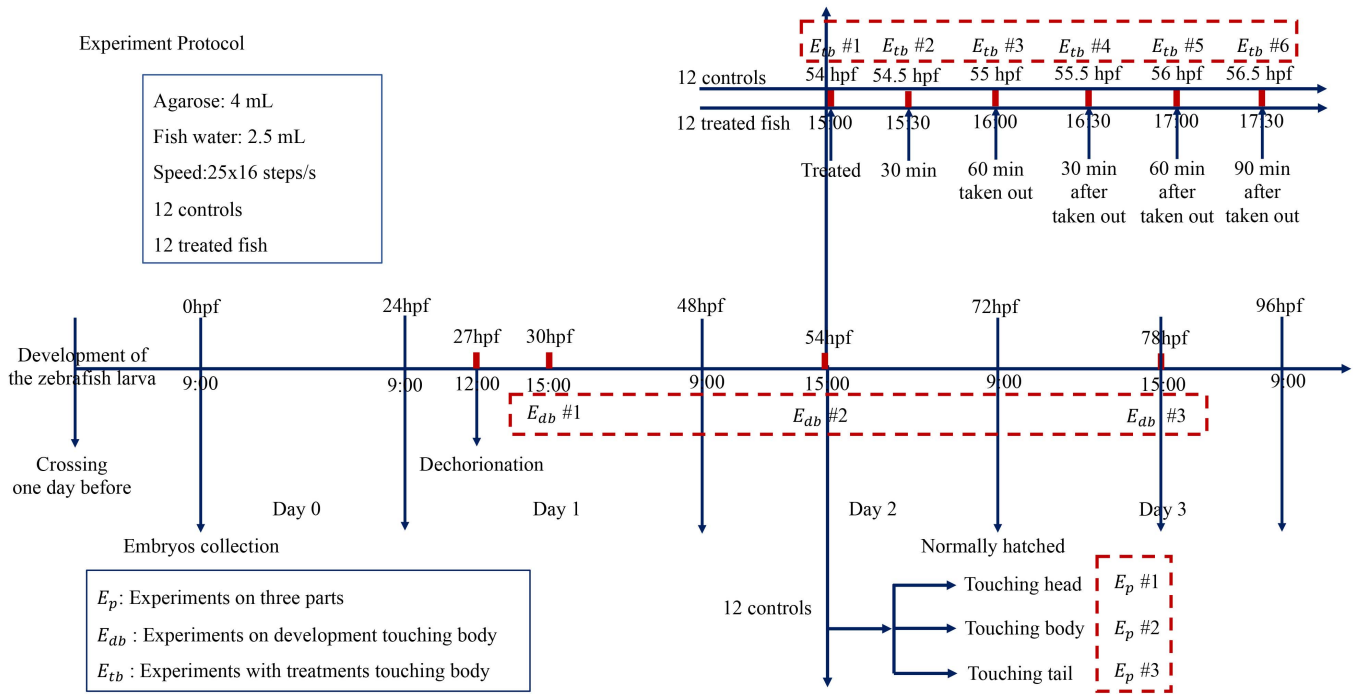

Fig. 11. Protocol of the verification experiments.

Appendix D
Behavior Quantification

A. Latency Time Analysis

The latency time t_l is defined as the difference of two time points: 1) the needle stops and touch begins at t_1 and 2) the first response of the larva begins at t_2. Since the detection method mentioned in Section II-C has risks of missing the needle and the larva, the positions of them should be tracked with the help of tracking procedure. Normally, without stimuli, the larva will keep stable and has not any response, so in the phase before touching, only the needle needs to be tracked. Moreover, the needle moves slightly without significant changes between frames, so the optical flow-based tracking procedure [35], [36] is suitable in this case. Optical flow is based on Taylor series, and the next position of the needle is estimated according to the gradients. Let $f\{x_o, y_o, t_i\}$ be the pixel value at the old needle position at frame i, and $f\{x_n, y_n, t_{i+1}\}$ be the pixel value at the new needle position at frame $i+1$, then the position change between these two frames is estimated as follows:

$$\begin{bmatrix} u \\ v \end{bmatrix} = \begin{bmatrix} \sum_i f_{x_i}^2 & \sum_i f_{x_i} f_{y_i} \\ \sum_i f_{x_i} f_{y_i} & \sum_i f_{y_i}^2 \end{bmatrix}^{-1} \begin{bmatrix} -\sum_i f_{x_i} f_{t_i} \\ -\sum_i f_{y_i} f_{t_i} \end{bmatrix} \tag{9}$$

$$x_i, y_i \in U\{x_o, y_o\}_{3\times 3}$$

$$f_x = \frac{\partial f}{\partial x}, \quad f_y = \frac{\partial f}{\partial y}, \quad f_t = \frac{\partial f}{\partial t} \tag{10}$$

$$u = \frac{dx}{dt}, \quad v = \frac{dy}{dt} \tag{11}$$

$$\{x_n, y_n\} = \text{argmin}\{f\{x_o + u, y_o + v, t_{i+1}\}\}_{7\times 7} \tag{12}$$

where u and v are the estimated changes in the x-axis and y-axis, respectively, and they are calculated according to the partial derivatives within a 3×3 adjacent area of the old needle position. The estimates from optical flow may miss the needle after the touching task, since the pixels around the needle may change a lot with the movement of the larva. Thus, we optimized the tracking strategy by finding the position with the lowest pixel value within a 7×7 adjacent area of the estimated needle position, as formulated in (12).

For the movement of the larva, unfortunately, optical flow is not useful as the larva has obvious changes to the touching. Thus, the difference method [seen in Fig. 12(a)] based on gradients, which could find the number of changing pixels of the larva, fits better to detect the movement of the larva. The percentage of these changing pixels in the larva area gives a clue of whether the larva begins to move, so we set T_m to be the threshold of moving. Basically, T_m is vital to the quantification results—too small value generates negative result and too large value generates only zero result—so to choose a suitable T_m, we changed it from 0% to 30% of the larva area and outlined the results of 12 controls (expected to have response, as pos) and 12 treated larvae (expected to have no response, as neg) at 54.5 hpf. After T_m was set at 20%, the pos showed clear results and the neg showed zero result, so 20% was chosen as T_m. According to the time points at which the needle stops and the response begins, the time difference $t_2 - t_1$ is the latency time t_l of the larva.

B. C-Bend Radius Average Analysis

The average radius of the C-Bends that larvae form conveys much information related to the amplitude of their touch response. The difference method mentioned above could give the positions of the moving larva as well as the area of it,

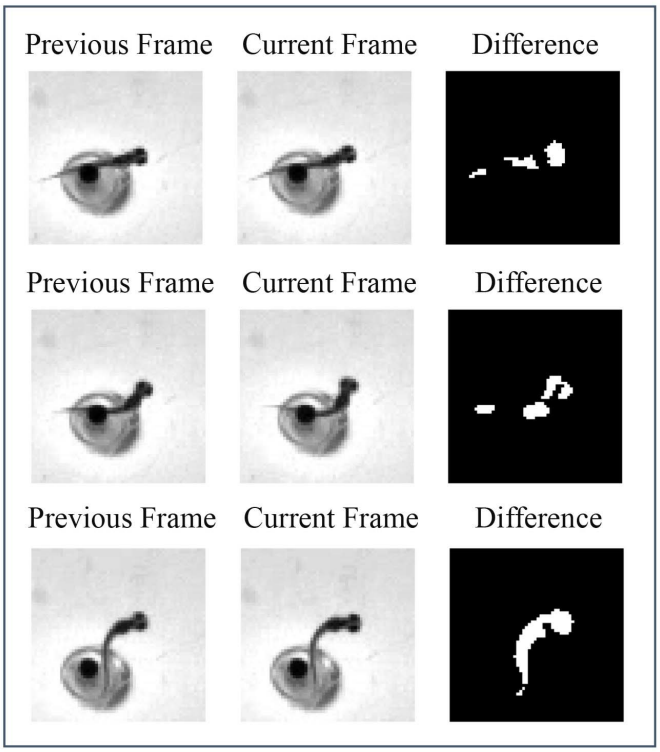

Fig. 12. Difference method and curve fitting method. (a) Response of the larva changed the pixels around in a considerable scale, causing a difference frame (the third picture in each row) between the previous (the first) and current (the second) frames. (b) Curve fitting includes three steps: binarization, skeleton detection, and iterated curve fitting (described in Algorithm 1). The fourth picture shows the third-order curve (in blue) fit by inliers after iterations, which is mapped to the original image patch in a green curve.

which could be cropped to detect the C-Bend. The skeleton of the larva was first extracted and an iterative curve fitting algorithm was used to compute the radius of the C-Bend in each frame. Assumed that there are totally n points along the skeleton and that a mth-order based curve should be fit, the algorithm of this iterated curve fitting comes as Algorithm 1 shows.

For each step of curve fitting, the least square method was used to optimize the variables $\{p_j\}_{j=1:m}$. Fig. 12(b) shows the result of one fit curve. This algorithm outputs the inliers of one C-Bend curve to compute the radius (by using also the least square method) and the C-Bend radius average was calculated by averaging all the radii.

C. Response Time and Moving Distance Analysis

The duration time (response time) and the total distance (moving distance) that the larva moves are also considered for the whole response. The difference method was applied to every frame of the video, detecting moving areas with the centers of their gravities. The sum of all the distances between these centers was computed as the larva's moving distance to touching, as similarly done for the response time t_r—by computing the time difference between the response begins at t_2 and ends at t_3.

Algorithm 1 Iterated Curve Fitting for C-Bend Detection and Radius Computation

Input: $\{X_i, Y_i\}_{i=1:n}$ (Skeleton points)
Initialization:
  $\{p_j = 0.1\}_{j=1:m}$
  $\epsilon \leftarrow 10$
  $threshold \leftarrow 2.5$
while $\epsilon > threshold$ **do**
  Optimize $\{p_j\}_{j=1:m}$
  $\hat{Y} \leftarrow p_0 + p_1 \times X + \cdots + p_m \times X^m$
  $\delta Y \leftarrow Y - \hat{Y}$
  $\epsilon \leftarrow max\{\delta Y_i\}_{i=1:n}$
  $I \leftarrow argmax\{\delta Y_i\}_{i=1:n}$
  if $\epsilon > threshold$ **then**
    remove$\{X_I, Y_I\}$
    $n \leftarrow n - 1$
  else
    break
  end if
end while
return $\{p_j\}_{j=1:m}$, with inliers of the curve

ACKNOWLEDGMENT

The authors would like to thank the program of BioInterfaces in Technology and Medicine (BIFTM) and the BioInterfaces International Graduate School (BIF-IGS) at the Karlsruhe Institute of Technology (KIT).

NOTES ON CONTRIBUTORS

Conceptualization and methodology, Y.W., D.M., R.P., and M.R.; experiments, validation, investigation, and visualization, Y.W., V.T., N.K.K, R.P., and M.R.; formal analysis and writing|original draft preparation, Y.W., R.P., and M.R.; writing|review and editing, Y.W., D.M. C.P., R.M., R.P., and M.R.; supervision and funding acquisition, Y.W., C.P., R.P., and M.R. All authors have read and agreed to the published version of the article.

REFERENCES

[1] D. Kokel *et al.*, "Rapid behavior-based identification of neuroactive small molecules in the zebrafish," *Nature Chem. Biol.*, vol. 6, no. 3, pp. 231–237, Mar. 2010.

[2] M. Granato *et al.*, "Genes controlling and mediating locomotion behavior of the zebrafish embryo and larva," *Development*, vol. 123, no. 1, pp. 399–413, Dec. 1996.

[3] Y. Naganawa and H. Hirata, "Developmental transition of touch response from slow muscle-mediated coilings to fast muscle-mediated burst swimming in zebrafish," *Develop. Biol.*, vol. 355, no. 2, pp. 194–204, Jul. 2011.

[4] T. E. Sztal, A. A. Ruparelia, C. Williams, and R. J. Bryson-Richardson, "Using touch-evoked response and locomotion assays to assess muscle performance and function in zebrafish," *J. Visualized Exp.*, vol. 116, Oct. 2016, Art. no. e54431.
[5] T. Pietri, E. Manalo, J. Ryan, L. Saint-Amant, and P. Washbourne, "Glutamate drives the touch response through a rostral loop in the spinal cord of zebrafish embryos," *Develop. Neurobiol.*, vol. 69, no. 12, pp. 780–795, Oct. 2009.
[6] L. Guzman *et al.*, "Evaluation of the effects of acetylcholinesterase inhibitors in the zebrafish touch-evoked response: Quantitative vs. Qualitative assessment," *Environ. Sci. Eur.*, vol. 32, no. 1, pp. 1–12, Dec. 2020.
[7] D. Kokel *et al.*, "Identification of nonvisual photomotor response cells in the vertebrate hindbrain," *J. Neurosci.*, vol. 33, no. 9, pp. 3834–3843, Feb. 2013.
[8] A. V. Kalueff *et al.*, "Towards a comprehensive catalog of zebrafish behavior 1.0 and beyond," *Zebrafish*, vol. 10, no. 1, pp. 70–86, Mar. 2013.
[9] R. C. Eaton and C. B. Kimmel, "Directional sensitivity of the Mauthner cell system to vibrational stimulation in zebrafish larvae," *J. Comparative Physiol. A*, vol. 140, no. 4, pp. 337–342, 1980.
[10] S. E. Brockerhoff, "Measuring the optokinetic response of zebrafish larvae," *Nature Protocols*, vol. 1, no. 5, p. 2448, 2006.
[11] W. Mo, F. Chen, A. Nechiporuk, and T. Nicolson, "Quantification of vestibular-induced eye movements in zebrafish larvae," *BMC Neurosci.*, vol. 11, no. 1, p. 110, 2010.
[12] Y. Gao *et al.*, "A high-throughput zebrafish screening method for visual mutants by light-induced locomotor response," *IEEE/ACM Trans. Comput. Biol. Bioinf.*, vol. 11, no. 4, pp. 693–701, Jul. 2014.
[13] D. Marcato *et al.*, "An automated and high-throughput photomotor response platform for chemical screens," in *Proc. 37th Annu. Int. Conf. IEEE Eng. Med. Biol. Soc. (EMBC)*, Aug. 2015, pp. 7728–7731.
[14] R. Candelier, M. S. Murmu, S. A. Romano, A. Jouary, G. Debrégeas, and G. Sumbre, "A microfluidic device to study neuronal and motor responses to acute chemical stimuli in zebrafish," *Sci. Rep.*, vol. 5, no. 1, p. 12196, Dec. 2015.
[15] A. C. Roberts *et al.*, "Rapid habituation of a touch-induced escape response in zebrafish (Danio rerio) larvae," *PLoS ONE*, vol. 14, no. 4, Apr. 2019, Art. no. e0214374.
[16] S. E. Low *et al.*, "TRPM7 is required within zebrafish sensory neurons for the activation of touch-evoked escape behaviors," *J. Neurosci.*, vol. 31, no. 32, pp. 11633–11644, Aug. 2011.
[17] L. Saint-Amant and P. Drapeau, "Time course of the development of motor behaviors in the zebrafish embryo," *J. Neurobiol.*, vol. 37, no. 4, pp. 622–632, Dec. 1998.
[18] G. B. Downes and M. Granato, "Supraspinal input is dispensable to generate glycine-mediated locomotive behaviors in the zebrafish embryo," *J. Neurobiol.*, vol. 66, no. 5, pp. 437–451, Apr. 2006.
[19] P. D. McClanahan, J. H. Xu, and C. Fang-Yen, "Comparing *Caenorhabditis elegans* gentle and harsh touch response behavior using a multiplexed hydraulic microfluidic device," *Integrative Biol.*, vol. 9, no. 10, pp. 800–809, 2017.
[20] Y. Cho, D. A. Porto, H. Hwang, L. J. Grundy, W. R. Schafer, and H. Lu, "Automated and controlled mechanical stimulation and functional imaging *in vivo* in C. elegans," *Lab Chip*, vol. 17, no. 15, pp. 2609–2618, 2017.
[21] Y. Cho, S. A. Lee, Y. L. Chew, K. Broderick, W. R. Schafer, and H. Lu, "Multimodal stimulation in a microfluidic device facilitates studies of interneurons in sensory integration in C. Elegans," *Small*, vol. 16, no. 10, 2020, Art. no. 1905852.
[22] A. L. Nekimken, B. L. Pruitt, and M. B. Goodman, "Touch-induced mechanical strain in somatosensory neurons is independent of extracellular matrix mutations in *Caenorhabditis elegans*," *Mol. Biol. Cell*, vol. 31, no. 16, pp. 1735–1743, Jul. 2020.
[23] C. L. Essmann *et al.*, "Mechanical properties measured by atomic force microscopy define health biomarkers in ageing C. elegans," *Nature Commun.*, vol. 11, no. 1, pp. 1–16, Dec. 2020.
[24] S.-J. Park, B. C. Petzold, M. B. Goodman, and B. L. Pruitt, "Piezoresistive cantilever force-clamp system," *Rev. Sci. Instrum.*, vol. 82, no. 4, Apr. 2011, Art. no. 043703.
[25] B. Ahmad, T. Kawahara, T. Yasuda, and F. Arai, "Microrobotic platform for mechanical stimulation of swimming microorganism on a chip," in *Proc. IEEE/RSJ Int. Conf. Intell. Robots Syst.*, Sep. 2014, pp. 4680–4685.
[26] C. B. Kimmel, W. W. Ballard, S. R. Kimmel, B. Ullmann, and T. F. Schilling, "Stages of embryonic development of the zebrafish," *Develop. Dyn.*, vol. 203, no. 3, pp. 253–310, Jul. 1995.
[27] P. Pichler and L. Lagnado, "The transfer characteristics of hair cells encoding mechanical stimuli in the lateral line of zebrafish," *J. Neurosci.*, vol. 39, no. 1, pp. 112–124, Jan. 2019.
[28] Y. Tomizawa, K. Dixit, D. Daggett, and K. Hoshino, "Biocompatible cantilevers for mechanical characterization of zebrafish embryos using image analysis," *Sensors*, vol. 19, no. 7, p. 1506, Mar. 2019.
[29] A. F. Mead, G. G. Kennedy, B. M. Palmer, A. M. Ebert, and D. M. Warshaw, "Mechanical characteristics of ultrafast zebrafish larval swimming muscles," *Biophys. J.*, vol. 119, no. 4, pp. 806–820, Aug. 2020.
[30] D. Marcato, "Design and development of imaging platforms for phenotypic characterization of early zebrafish," Ph.D. dissertation, Karlsruher Institut Für Technologie (KIT), Karlsruhe, Germany, 2018. Accessed: Aug. 6, 2018.
[31] S. A. Budick and D. M. O'Malley, "Locomotor repertoire of the larval zebrafish: Swimming, turning and prey capture," *J. Exp. Biol.*, vol. 203, no. 17, pp. 2565–2579, 2000.
[32] T. W. Dunn *et al.*, "Neural circuits underlying visually evoked escapes in larval zebrafish," *Neuron*, vol. 89, no. 3, pp. 613–628, Feb. 2016.
[33] J. Duan *et al.*, "Toxic effects of silica nanoparticles on zebrafish embryos and larvae," *PLoS ONE*, vol. 8, no. 9, Sep. 2013, Art. no. e74606.
[34] T. Atherton and D. J. Kerbyson, "Size invariant circle detection," *Image Vis. Comput.*, vol. 17, no. 11, pp. 795–803, Sep. 1999.
[35] B. K. Horn and B. G. Schunck, "Determining optical flow," *Proc. SPIE*, vol. 281, pp. 319–331, Nov. 1981.
[36] T. Senst, V. Eiselein, and T. Sikora, "Robust local optical flow for feature tracking," *IEEE Trans. Circuits Syst. Video Technol.*, vol. 22, no. 9, pp. 1377–1387, Sep. 2012.

Yanke Wang received the bachelor's and master's degrees in automation from Harbin Engineering University, Harbin, China, in 2017 and 2019, respectively.

Since 2019, he is a Doctoral Researcher with the Faculty of Mechanical Engineering and is working in the research group "Machine Learning for High-Throughput and Mechatronics" with the Institute for Automation and Applied Computer Science, Karlsruhe Institute of Technology, Karlsruhe, Germany. His research interests include automated systems, bio-informatics, data science, computer vision, and machine learning.

Daniel Marcato received the Dipl.-Ing. degree in bioengineering and the Ph.D. degree in mechanical engineering with a focus on applied computer science from the Karlsruhe Institute of Technology, Karlsruhe, Germany, 2013 and 2018, respectively.

He joined DITABIS AG in 2017 as Systems Engineer with the Research & Development Department where he is involved with the development of innovative medical devices. He has been working on automated solutions for zebrafish research since 2014 and is currently responsible for the technological development of the high-throughput microscope acquifer imaging machine.

Vani Tirumalasetty received the bachelor's degree in genetic engineering from SRM University, Kattankulathur, India, in 2019, and did her bachelor thesis project in Molecular Biology and Developmental Genetics at Tzu Chi University, Hualien, Taiwan, in 2019. Since 2020, she is pursuing the master's degree in geobiology and paleobiology at Ludwig Maximilian's University, Munich, Germany.

She has worked as a Scientific Assistant at IBCS-BIP at Karlsruhe Institute of Technology, Karlsruhe, Germany. Her primary interest lies in developmental and evolutionary genetics studies.

Naveen Krishna Kanagaraj received the bachelor's degree in genetic engineering from SRM Institute of Science and Technology, Kattankulathur, India, in 2019.

Since 2019, he is working as a Scientific Assistant at the Screening Center, Institute of Biological and chemical Systems–Biological Information Processing, Karlsruhe Institute of Technology, Karlsruhe, Germany. His research interests include developmental genetics, neuroscience, gene–brain-behavior coordination, and imaging techniques.

Christian Pylatiuk received the M.D. degree from the University of Marburg, Marburg, Germany, in 1997.

Since 2014, he is an Adjunct Professor with the Faculty of Mechanical Engineering, Karlsruhe Institute of Technology, Karlsruhe, Germany, for "Medical Technology." His research interests include mechatronics, medical technology, medical automation, and image analysis.

Ralf Mikut received the Dipl.-Ing. degree in automatic control from the University of Technology, Dresden, Germany, in 1994, and the Ph.D. degree in mechanical engineering from the University of Karlsruhe, Karlsruhe, Germany, in 1999.

Since 2011, he is an Adjunct Professor with the Faculty of Mechanical Engineering and Head of the Research Group Automated Image and Data Analysis at the Institute for Automation and Applied Informatics, Karlsruhe Institute of Technology (KIT), Karlsruhe, Germany. His current research interests include machine learning, image processing, life science applications, and smart grids.

Ravindra Peravali received the bachelor's degree of engineering in electronics and communications engineering from the University of Mysore, Mysore, India, in 1993, the M.S. degree in electrical engineering from the University of Maryland, Baltimore County, Baltimore, MD, USA, in 1997, and the Ph.D. degree in biosciences from Heidelberg University, Heidelberg, Germany, in 2018.

He is currently the Head of the Screening Center at the Institute of Biological and Chemical Systems–Biological Information Processing, Karlsruhe Institute of Technology, Karlsruhe, Germany. His research interests are in understanding the neural mechanisms involved in animal behavior using zebrafish and Medaka as model organisms. In addition, he works in high-throughput imaging and in mathematical modeling of biological information.

Markus Reischl received the Dipl.-Ing. and Ph.D. degrees in mechanical engineering from the University of Karlsruhe, Karlsruhe, Germany, in 2001 and 2006, respectively.

Since 2020, he is an Adjunct Professor with the Faculty of Mechanical Engineering and is heading the research group "Machine Learning for High-Throughput and Mechatronics" with the Institute for Automation and Applied Computer Science, Karlsruhe Institute of Technology, Karlsruhe, Germany. His research interests include man–machine interfaces, image processing, machine learning, and data analytics.